# DIRC Note #141

May 23, 2001

Internal Group Note

(Revision on Feb. 19, 2003)

# Photon Background in DIRC Fused Silica Bars

K. Yarritu, S. Spanier and J. Va'vra

## Abstract

We show that the scintillation mechanism is negligible in fused silica; it represents less than 1% of two other major components in the photon background. One such component consists of photons created by the delta ray electrons in the fused silica, which in turn can produce Cherenkov light. The second component comes from the reflections of photons from the EPOTEK-301-2 glue/fused silica interface. The reflection occurs because of a slight mismatch of the refraction index between the optical glue and the fused silica. The note will be useful to estimate the photon background multiplicity and provides a recipe how to simulate it in the BaBar Monte Carlo for each passing minim ionizing particle through the DIRC [1] bar. This is a new version of the same note, dated September 19, 2001, and it contains some improvements in the Monte Carlo simulation (see Section 6.2).

## 1. Introduction

The background in the fused silica bars has been studied several times [2,3]. It has been argued that there are two dominant contributions: the delta ray initiated radiative processes and the scintillation mechanism. It was also suggested that there is also a third component, which is caused by the randomly scattered Cherenkov photons on the bar imperfections, i.e., it depends on the quality [2].

Our study confirms that the delta ray contribution is indeed very significant process. However, we show that the scintillation mechanism is negligible in fused silica. Instead, the second dominant component comes from the reflections of photons from the EPOTEK-301-2 glue/fused silica interfaces. Although the reflection coefficient is relatively small, the effect is significant because one deals with a very large number of the Cherenkov photons at large dip angles (easily more than 1000 photons can bounce in the bar). We offer these arguments in favor of our interpretation of the background:

- The direct measurement of the scintillation in the bar measurement with the $Fe^{55}$ X-ray source placed directly on the bar surface shows a small rate of the photon activity in the bar, which cannot explain the measured rate of the background photons in the 4m-long bar tests.
- The measured rate of the photon background generated by cosmic ray muons in the 4m-long bar test, presented in this paper, can be explained with just two dominant processes present on the Monte Carlo program: delta rays and reflections from the glue joints. The 4m-long bar measurement "separates" the background photons from the Cherenkov signal photons in time by choosing a large incident muon angle relative to the bar axis so that all Cherenkov signal photons travel away from the PMT. When the bar is equipped with a mirror, there is about 30ns available to study the background time structure before a large Cherenkov signal returns to the PMT. When the bar has a photon trap, the Cherenkov signal disappears completely and one has a time window of about 70ns to study the background.
- With a detailed Monte Carlo simulation we explain the photon background in the cosmic ray muon test with the 4m-long bar. This program uses the Fluka generator of delta-electrons, and includes effects such as the multiple scattering of the delta rays, the Fresnel reflection on the fused silica/glue interface including the polarization effect, etc.
- The measurement of the EPOTEK-301-2 refraction index and a direct measurement of the reflection from the glue/fused silica interface [see Ref. 4 for details]. This improves our knowledge of the refraction index compared to information from the Epotek Co., which was used in Ref. 5.

## 2. Refraction Index of EPOTEK-301-2 Glue and the Fresnel Reflection.

Ref. 4, motivated by the present work, provided the measurement of the refraction index of the EPOTE-301-2 glue, and also a direct measurement of the reflectivity of the EPOTEK-301-2 glue/fused silica interface. In this paper, we present only a summary of this study. Figure 1 shows the EPOTEK refraction index [4] together with similar fits to data of fused silica and water. Based on this result, one can calculate the Fresnel reflection on the EPOTEK-301-2 glue/fused silica interface. Figure 2 shows an example of such calculation as a function of incident angle for two laser polarizations at 442nm.

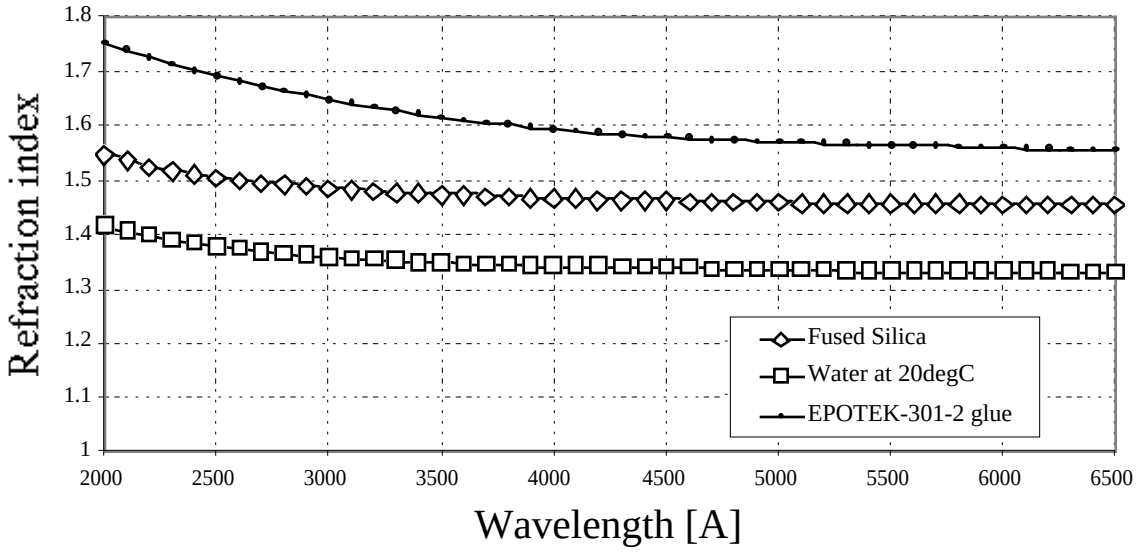


Fig. 1 – Refraction index of fused silica[1], water[2] and EPOTEK-301-2 optical glue[3] used to glue DIRC bars together.

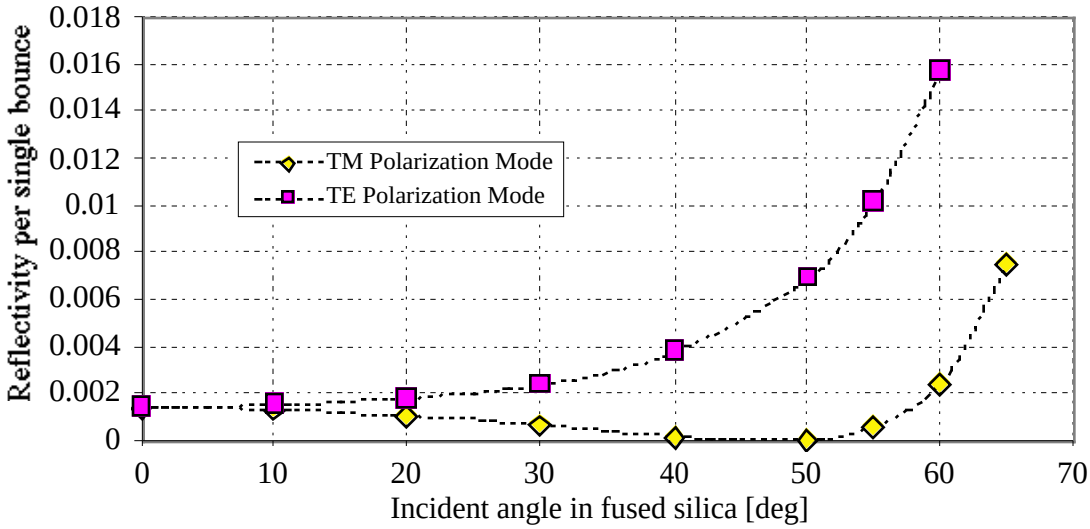


Fig. 3 – Fresnel reflectivity per single bounce from the EPOTEK-301-2 glue / fused silica interface for TE and TM photon polarization modes (calculated at 442 nm). The calculation is based on the knowledge of the refraction index only.

[1] This parameterization of the quartz refraction index comes from the Melles-Griot Company's catalog.
[2] The refraction index data come from N.I. Koshkin, M.G. Shirkevich, Handbook of Elementary Physics, 1982.
[3] Fit to the refraction index data presented in Ref. 4.

In principle, the measurement of the refraction index of fused silica and the glue as a function of wavelength is sufficient to calculate the reflectivity according to the Fresnel theory. Nevertheless, Ref. 4 measured this reflectivity directly at 442nm and obtained somewhat surprising result. The measured reflectivity was significantly higher than what was predicted by the Fresnel theory. Figure 3 shows the result. It is not presently clear why the reflection from this interface seems to be more complicated than the theory would suggest. The Monte Carlo program, used to explain the 4m-ling bar test data, agrees with the Fresnel prediction up to an angle of ~50º, as one can see in Fig. 3 (see more details in chapters 4 and 5).

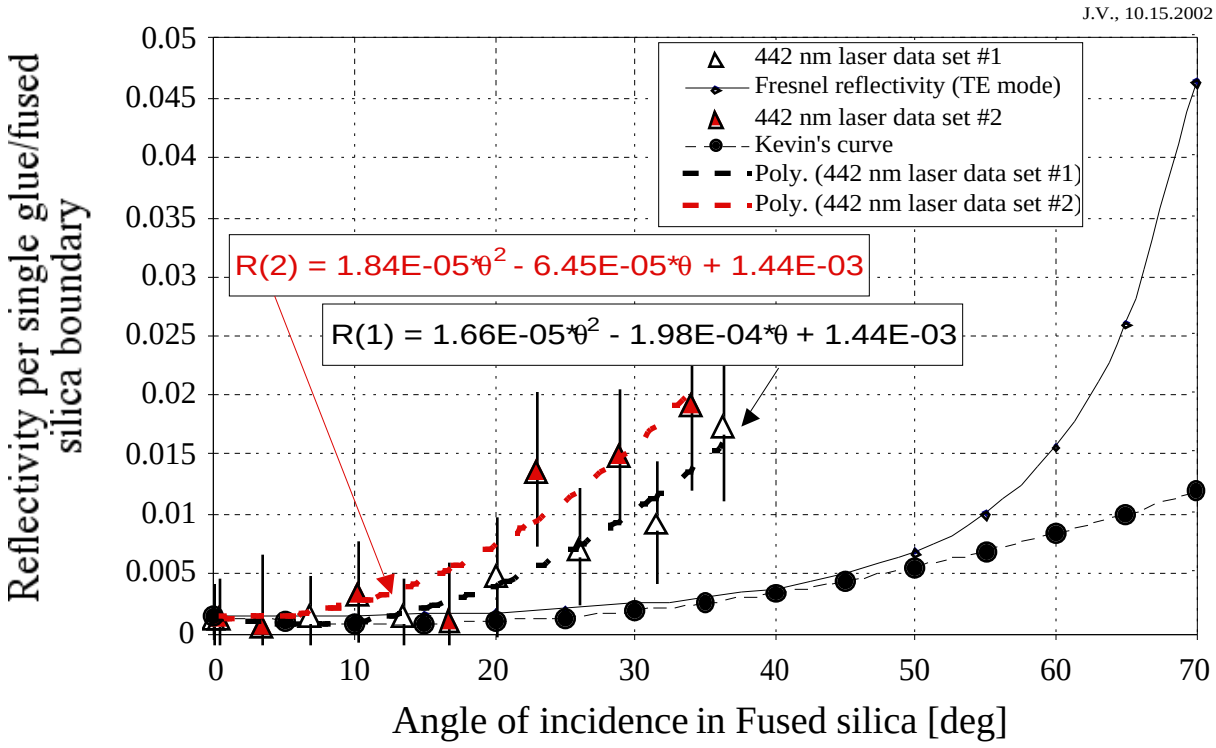


Fig. 3 – Fit two different direct measurements of the reflectivity per single bounce from the EPOTEK-301-2 glue/fused silica interface. The graph also shows the Fresnel reflectivity curve, which is based on the measurement of the EPOTEK-301-2 glue refraction index [4], and also the Monte Carlo curve, which is used to explain the 4m-long bar photon background data in this paper (see chapter 5). It agrres with the Fresnel up an angle of about 50º.

## 3. Measurement of Scintillation in DIRC Fused Silica Bar.

The most direct and cleanest way to look for the scintillation in fused silica is, perhaps, to use the $Fe^{55}$ source, which emits 5.9 keV X-rays primarily. Its contamination by more energetic Gamma rays[1] is negligible (probability of less than $1.28 \times 10^{-7}$). The Gamma rays would produce the Compton electrons, which can have enough energy to be above the Cherenkov threshold, and this would confuse the photon counting results of this particular study. On the other hand, the 5.9keV X-rays from the $Fe^{55}$ source can create scintillation photons only via the photoeffect mechanism in fused silica. The photoeffect ($\gamma$ + " bound $e^-$" --> " free $e^-$") produces a soft electron (~5.9keV) with enough energy to only excite nearby atoms, which can then emit scintillation photons, infrared photons, phonons, etc. Our photomultiplier detector can detect only scintillation photons of energy between 300 and 800nm. The photons outside of this energy range are not detected. The same applies to the BaBar DIRC photon detector. The electron energy is of a similar magnitude as average dE/dx excitations by a

[1] The Lund/LBNL Nuclear Data http://nucleardata.nuclear.lu.se/nucleardata/toi/index.asp. The $Fe^{55}$ source small contamination of Gamma rays, produced by electron capture, have energy of 125.95 keV (probability of less than $1.28 \times 10^{-7}$).

fast particle, and therefore we think the $Fe^{55}$ source simulates the problem reasonable well. There are many other sources of soft X-rays, for example Cu, Rb, Mo, Ag, Ba and Rb. Unfortunately, they are not useful for our scintillation study because all these sources have a substantial contamination from more energetic Gamma rays produced in parallel to softer X-ray production.

The calculated external activity at the $Fe^{55}$ source exit window, in terms of the $E_\gamma$ = 5.9keV X-rays, is calculated to be $R_o$ ~$3.6x10^7$ counts/min, based on the source age (~12 years), its initial activity when purchased (20mC), and a knowledge of the detailed geometry of the source. The $Fe^{55}$ source was placed directly on the DIRC fused silica bar surface (no absorber in between), and the observed background-subtracted signal rate in PMT was $R_s$ ~ (1.96±0.2) x $10^3$ counts/min – see Fig. 4. We assume that this rate is caused entirely by the scintillation mechanism in fused silica, and that its production is isotropic. According to the Monte Carlo simulation the PMT acceptance is ~5%. Therefore, the detector-independent probability that a single 5.9keV X-ray entering the DIRC fused silica bar will produce a scintillation photon is [$(1.96x10^3/3.6x10^7)/0.05$] ~$1.1x10^{-3}$. It is a small number but certainly not zero.

The question is how does the scintillation mechanism using the 5.9 keV X-rays relate to that of a passing muon through the fused silica bar. In the absence of a more sophisticated dE/dx model, one possible method is to make the relation using energy equivalence. From the measured scintillation rate of ~(1.96±0.2) x $10^3$ counts/min one can determine the scintillation rate per deposited energy of {[$(1.96x10^3/0.05)$ c/min] / ($3.6x10^7$ counts/min x 0.0059 MeV) ~1.8 x $10^{-1}$ counts/MeV. The minimum ionizing muon leaves about 13.5MeV when passing the bar at ~56.5° angle. Therefore, based on the equivalent energy argument, one expects about [(13.5 MeV x 1.8 x $10^{-1}$ counts/MeV)*0.05] ~0.12 detected scintillation photons per one passing muon. We actually detect 4.6 ± 1.8 background photons in total in the time window of 0-70ns per muon at ~56.5° angle (see measurements with the photon trap in chapter 4).

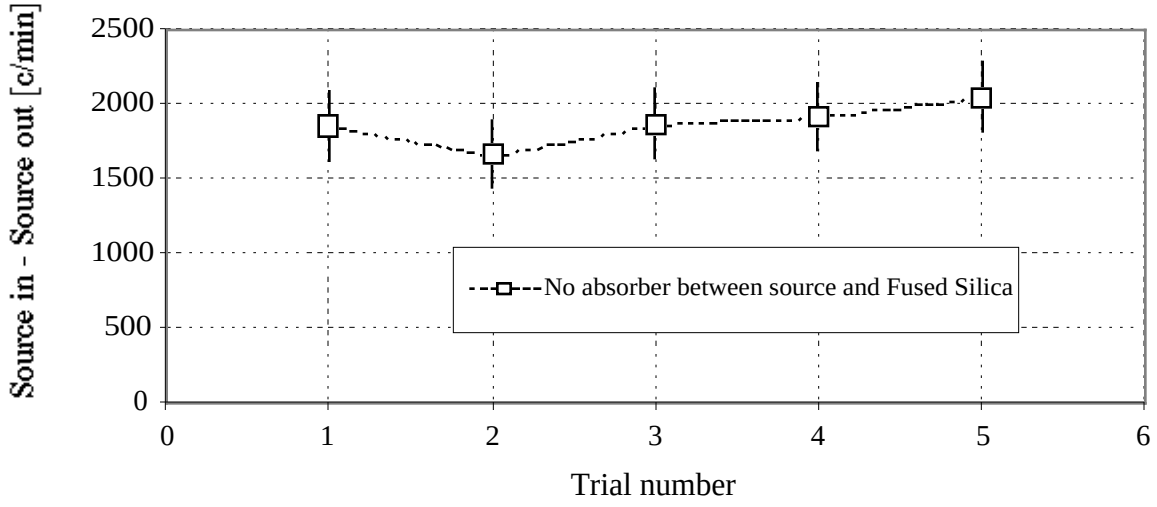


Fig. 4 - Observed background-subtracted PMT signal rate attributed to the scintillation mechanism in fused silica DIRC bar. The $Fe^{55}$ source is placed directly on the DIRC fused silica bar surface (no absorber).

## 4. Measurement of the Photon Background using the Cosmic Ray Muons.

The measurement is an indirect one. We want to "isolate" the background photons from the Cherenkov signal photons, and simulate the background component with the Monte Carlo. The best method to separate the two groups of photons is by time measurement. This is achieved by choosing a large incident muon angle relative to the bar axis so that all Cherenkov photons travel away from the PMT towards the mirror – see Fig. 5. When a bar is equipped with the mirror, one has about 30ns available to study the background time structure before a large Cherenkov signal returns. On the other hand, when a bar has the photon trap, the Cherenkov signal disappears completely and one has a time window of about 70ns to study the background activity. Our

Monte Carlo program has many new features compared to the standard DIRC Monte Carlo program. These include the proper treatment of the glue/fused silica interfaces, the delta ray generation using the FLUKA program, the multiple scattering of delta ray electrons, Cherenkov photon polarization, etc.

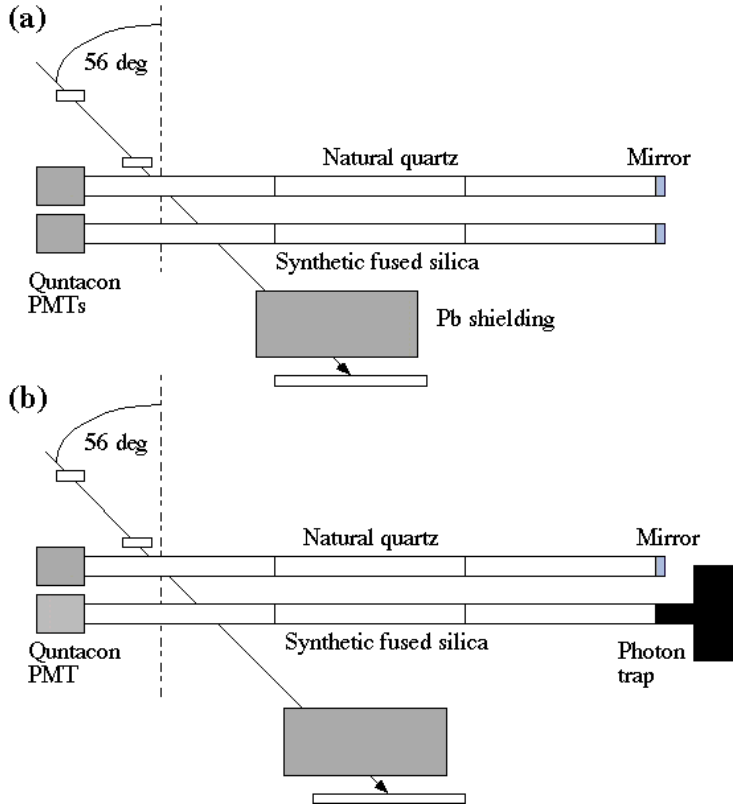


Fig. 5 – Experimental setup used to study the photon background. The Cherenkov signal propagates forward to either (a) a mirror or (b) the photon trap. In the former case, a window of ~30ns is available to study the "early" photon background activity before the Cherenkov signal returns; in the latter case a 70ns window is available. The lead shield is ~12" thick. Top bar had also a veto counter to eliminate cosmic ray showers. Picture is not to scale.

Figure 5 shows schematically the experimental arrangement to study the photon background using the cosmic ray muons in the natural quartz and the synthetic fused silica bars, located directly above each other. The particle trajectory is defined by two entrance scintillation counters limiting the angular acceptance to ± 5 degrees with respect to the mean of 56.5 degrees. The natural quartz material is Vitrosil type. The full size bar is glued together from three bars with dimensions ~15 x ~46 x ~1200 mm. The synthetic fused silica bar material is identical to BaBar DIRC bars. The full size bar is produced by gluing three individual bars with dimensions ~17 x 31.86 x ~1220 mm (Bars #247, 248 and 249 from the DIRC production). These bars are nearly perfect in terms of chips, scratches, etc. The Quantacon XP2020 Philips PMT was attached directly to the bar with the EPOTEK-301-2 glue. In the Monte Carlo program we simulate the PMT's end as a composition of four interfaces: (a) fused silica bar's end, (b) EPOTEK-301-2 glue, (c) Borosilicate glass and (d) bi-alkali photo-cathode with their respective refraction indices. The bars were glued following procedure as the DIRC production, i.e., the EPOTEK-301-2 glue thickness was 0.001" thick. The mirror was just air coupled with a spring applying a pressure, as is done in the DIRC. Initially, both bars were equipped with the mirrors. The Cherenkov signal was therefore reflected back to PMT, allowing to study the photon background for 30ns after a passage of cosmic ray muon.

For some portion of the run, the synthetic bar was connected to a photon trap, which entirely absorbed the Cherenkov signal. The photon trap is shown in Fig. 6. This allowed extending the length of the time window to 70ns and estimating the total rate of the background photons.

The PMTs signal was first amplified 10x with LeCroy fast PMT amplifier. Its output was digitized with the HP digital scope, which was read out by a MAC IIcx computer with the CAMAC-based GPIB interface. The on-line program was Fortran-based, the off-line analysis used a PAW-based programming. We applied a sophisticated pulse finding algorithm using several methods: (a) a simple peak finding method, (b) peak finding with the mathematically correct de-convolution algorithm, and (c) a software-based leading edge "single hit" algorithm. The simple peak finding method discarded the single photon pulse shape and just followed the waveform contour. The de-convolution algorithm took into account the correct single photon pulse shape. In addition, the hardware used LeCroy TDC, which allowed one to make a simple leading edge "single hit" measurement, which was compared to the software-based leading edge "single hit" algorithm.

Fig. 6 – Photon trap at the end of 4 meter-long synthetic fused silica bar. The aluminum container, filled with a fused silica matching fluid, is coupled to a bar via a pipe equipped with a rubber seal. The aluminum container and pipe walls are covered with a photon absorbing cloth. The trap was very efficient eliminating the entire Cherenkov signal.

## 4.1. Measurement with Bar made of DIRC Fused Silica Material.

### 4.1.1. Fused Silica Bar with a Mirror.

Figure 7 shows typical digital scope waveforms recorded by the experiment when both bars were equipped with the mirrors. One clearly sees a large Cherenkov signal on both traces (top trace corresponds to the natural quarz, the bottom trace to the synthetic fused silica). One also clearly sees the photon background in front of the Cherenkov signal. One has only 30ns available to study the background in this case. The background consists of tightly overlapping pulses, which requires a waveform analysis treatment. The simple peak finding algorithm follows a waveform channel by channel and finds a peak if the waveform starts dropping for at least 5 consecutive channels. Figure 8a shows the time distribution of pulses found with the simple peak finding method.

The Cherenkov peak appears at the scope channel ~150. The very first peak near channel ~115 correspond to the delta ray electrons traveling fast enough to produce the Cherenkov signal. A shoulder near channel ~130 corresponds to photons reflecting from the very first bar-to-bar glue joint; the bump near channel ~150 corresponds to the second glue joint. A three bin-wide "hole" just prior to channel ~150 is an artifact of imperfect pulse finding algorithm trying to avoid counting the huge Cherenkov signal. Figure 8b shows the time distribution using the single hit threshold software-based time finding algorithm. In this case the differentiation

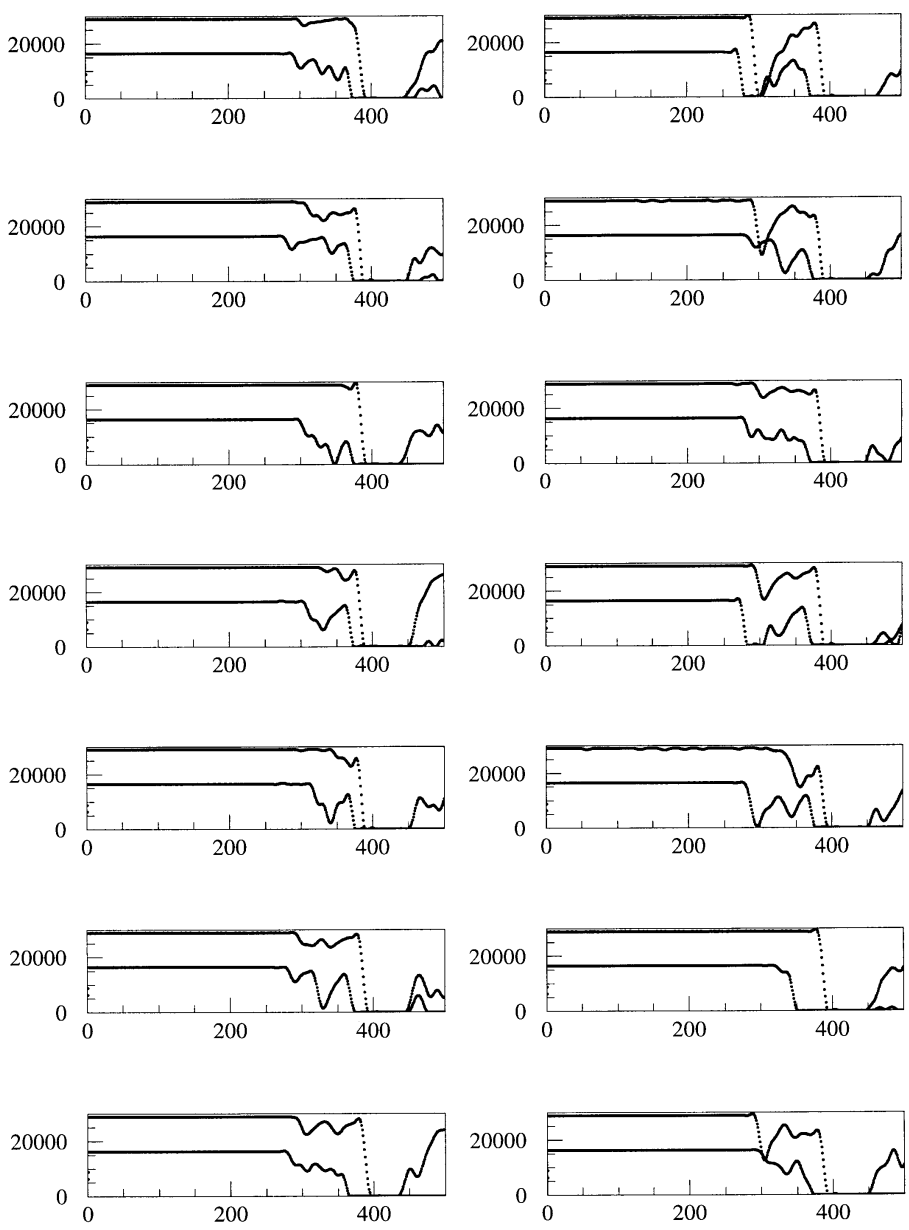


Fig. 7 – Mirror data only: Raw scope PMT of the background photon pulses from muons passing through the natural quartz bar (top scope traces) and fused silica bar (bottom scope traces). The angle of the track is such that all Cherenkov photons travel first away from the PMT, which allows to see a background photon activity before a saturating Cherenkov signal comes back from the mirror reflection. One has about ~30ns to perform a meaningful pulse finding algorithm to measure the background. The horizontal axis is time in terms of scope channels (1 scope channel = 0.4 ns) and the vertical axis is the amplitude.

between various background contributions is even more apparent. It is interesting to compare the software-based time distribution of Fig. 8 with the hardware single hit time distribution using the LeCroy TDC, shown on Fig. 9. Figure 9a corresponds to a 35mV threshold on the PMT amplifier discriminator, Figure 9b corresponds to a 300mV threshold. In the latter case, we detect only large pulses, which are the Cherenkov signal pulses

arriving ~30ns after the first delta-ray signal. One clearly recognizes the similar features between the hardware and software-based spectra, the most dominant feature being that the second peak follows the first one by ~15ns; the second peak corresponds to the reflection from the first bar-to-bar joint. However, the relative strength of individual contribution depends on the discriminator threshold, as is clearly seen comparing Figures 9a and 9b. The natural quartz data show similar features. The de-convolution algorithm will be discussed in the next chapter.

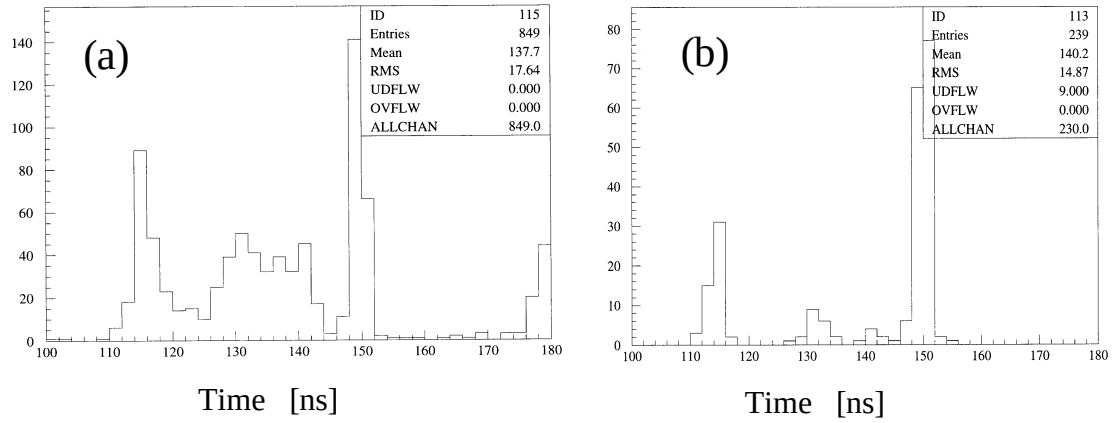


Fig. 8 – Mirror data only: measured time distribution of the background photon pulses obtained from the synthetic fused silica bar using (a) a simple peak finding algorithm, and (b) a simple "single hit" leading edge threshold algorithm. The Cherenkov return signal, reflected from the mirror, appears near channel 150 in both cases.

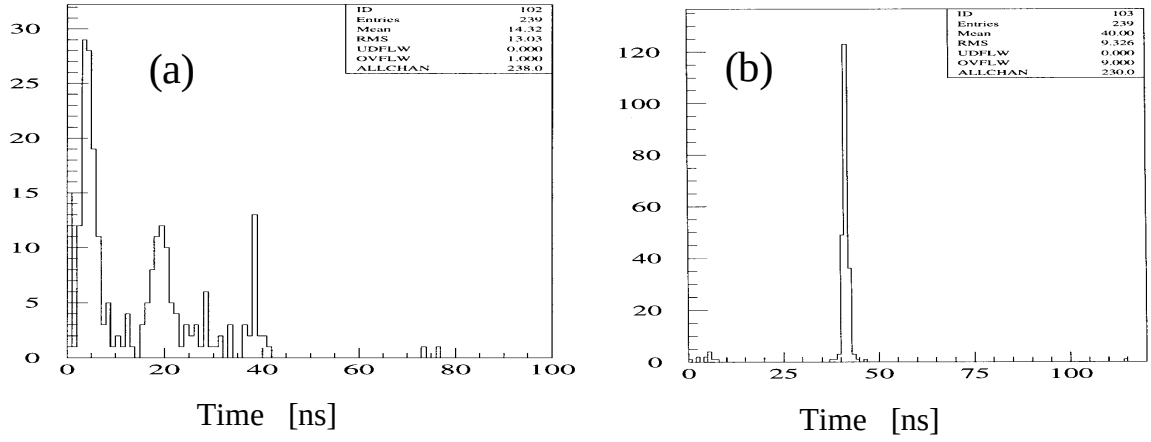


Fig. 9 – Mirror data only: measured time distribution of the background photon pulses obtained from the synthetic bar using the single hit LeCroy #2229 TDC. The PMT amplifier pulse was discriminated with a threshold of (a) 30mV (lowest possible) and (b) 300mV. In the latter case one detects mainly large Cherenkov pulses reflected from the mirror.

### 4.1.2. Fused Silica Bar with a Photon Trap.

The photon trap, shown in Fig. 6, proved to be a very effective tool to kill the Cherenkov signal traveling in the direction away from the PMT. Figure 10a shows the measured raw scope waveforms. One can easily notice the absence of otherwise dominant Cherenkov signal. Figure 10b shows the de-convoluted waveforms. The de-convolution algorithm assumes a standard PMT's amplifier pulse shape of a form $t*\exp(-t/\tau)$, where the shaping constant $\tau$ is assumed to be 20ns. The method converts the raw scope waveform into the de-convoluted one using the following equation:

$$d_i = r_i - 2\,e^{-T/\tau}\,r_{i-1} + e^{-2T/\tau}\,r_{i-2}$$

where T is the scope sampling time (0.4ns), $r_i$ is the i-th PMT output sample, and $d_i$ is the i-th de-convoluted sample. The de-convoluted waveform is then subject to a threshold cut to eliminate the unwanted noise pulses. Figure 10 also shows the peak values found by both the simple-minded peak finding and the de-convolution method. One can see that both methods agree on average, perhaps, in more busy regions the de-convolution method may do slightly better.

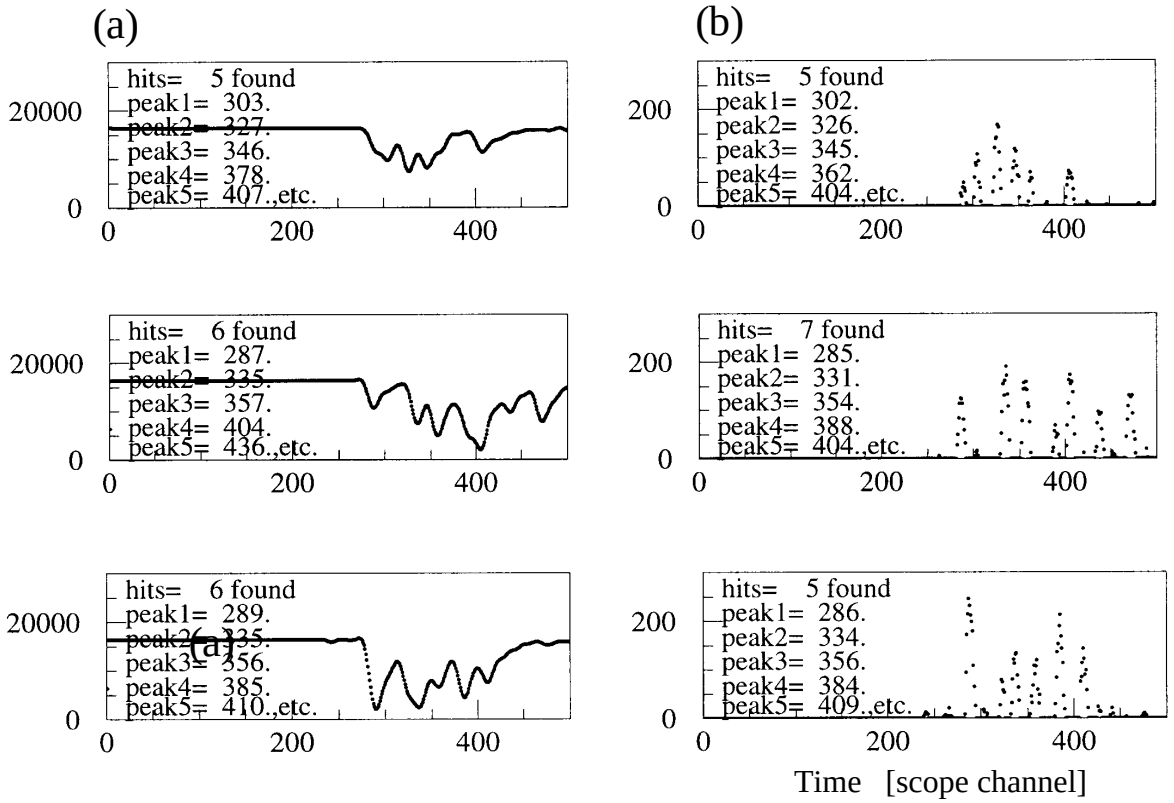


Fig. 10 – Photon trap data only: Raw digital scope PMT of the background photon pulses from muons passing through the synthetic fused silica bar (bottom scope trace in Fig. 7). All Cherenkov signal photons are absorbed in the photon trap, which enables one to study what otherwise would be under the Cherenkov peak, which gives a total range of ~70ns. Figure demonstrates the pulse finding method using (a) a simple peak finding algorithm, or (b) a peak finding using the pulse de-convolution algorithm. The horizontal axis is time in terms of scope channels (1 scope channel = 0.4 ns) and the vertical axis is amplitude. Figure shows numbers indicating how many and where the algorithms found the peaks.

Figure 11a shows the time distribution using the de-convoluted peaks. One notices the absence of the dominant Cherenkov signal, and one can notice that the measured background rate is slowly diminishing as one approaches the end of the 70ns time window. Again, one clearly recognizes the first, the second and the hint of the third peak, corresponding to the delta rays, the first and the second bar-to-bar joints. Figure 11b shows the time distribution using the single hit threshold software-based time finding algorithm. The second peak, corresponding to the reflection from the bar-to-bar interface is again clearly visible. Figure 12 shows the hardware single hit time distribution using the LeCroy #2229 TDC, where Fig. 12a corresponds to a 30mV threshold on the PMT amplifier discriminator, and Fig. 12b corresponds to a 300mV threshold. Again the second peak is clearly visible. Notice the absence of the Cherenkov signal in Fig. 12b between 35-40ns, which confirms a very good efficiency of the photon trap.

Figure 13a shows the multiplicity distribution of background photon pulses found in the time window 0-70ns for the synthetic fused silica bar equipped with the photon trap and using the simple peak finding

algorithm, Figure 13b shows the same for the de-convolution algorithm. Figure 14a shows the distribution of total number of pulses found in the time window 0-30ns for the natural quartz bar equipped with the mirror using the de-convolution algorithm. Figure 14b shows the same for the synthetic fused silica bar. Table 1 summarizes these results. One can see that we measure about five background photons in a 70ns time window. In the first 30ns, we typically detect about two background photons.

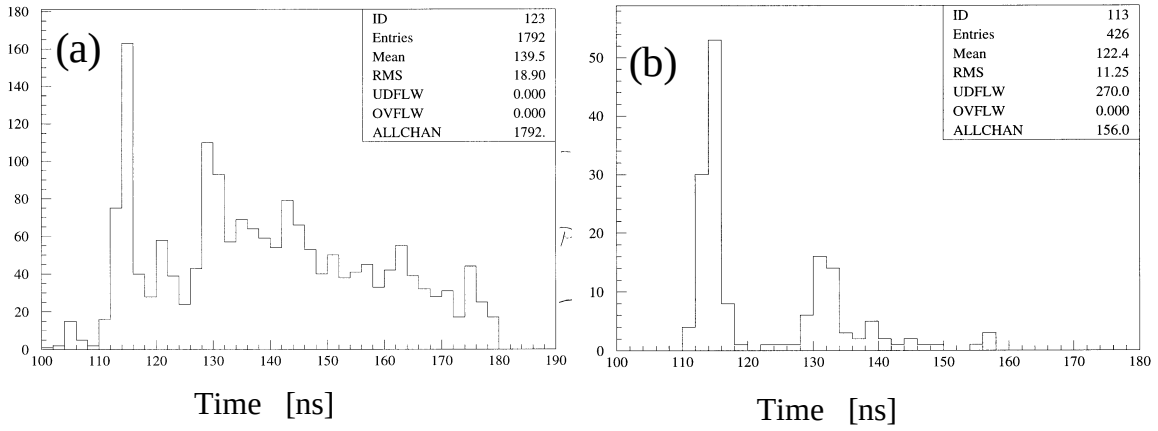


Fig. 11 – Photon trap data only: measured time distribution of the background photon pulses obtained from the synthetic fused silica bar using (a) the de-convolution algorithm, and (b) a simple "single hit" leading edge threshold algorithm. Notice the absence of the Cherenkov signal near channel 150.

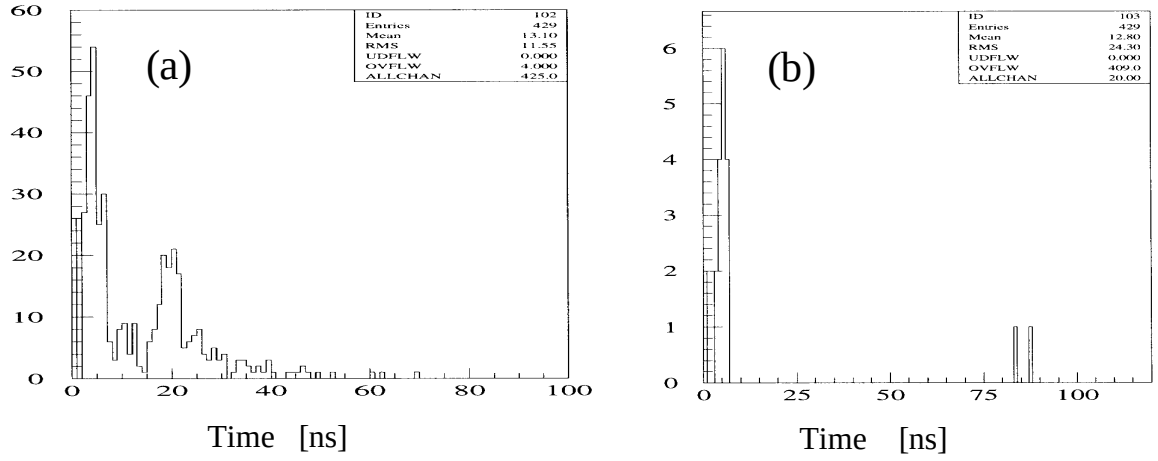


Fig. 12 – Photon trap data only: measured time distribution of the background photon pulses obtained from the synthetic bar equipped with the photon trap and the single hit hardware LeCroy TDC 2229. The PMT amplifier pulse discriminator was set to (a) a low value of 30mV and (b) a high value of 300mV.

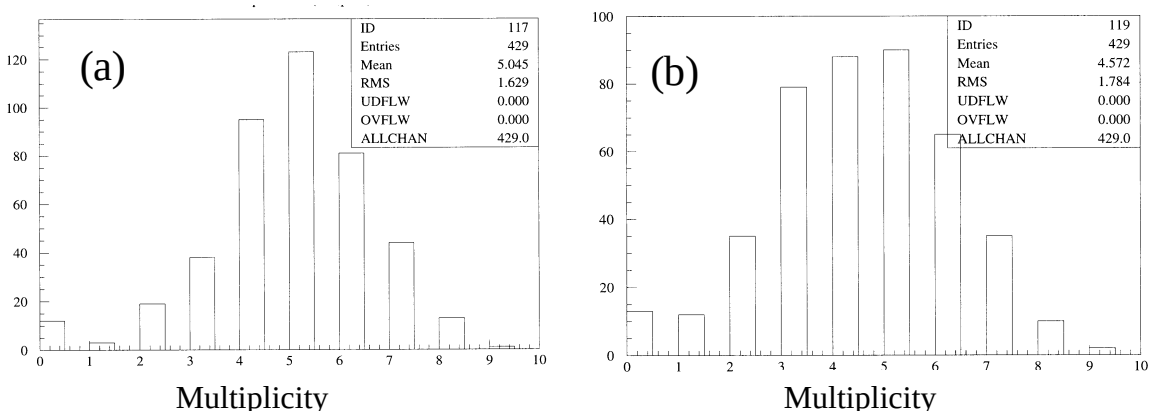


Fig. 13 – Photon trap data only: measured multiplicity distribution of the background photon pulses found in the synthetic fused silica bar in the time window of 0-70ns using (a) the simple minded peak finding algorithm, and (b) the de-convolution algorithm.

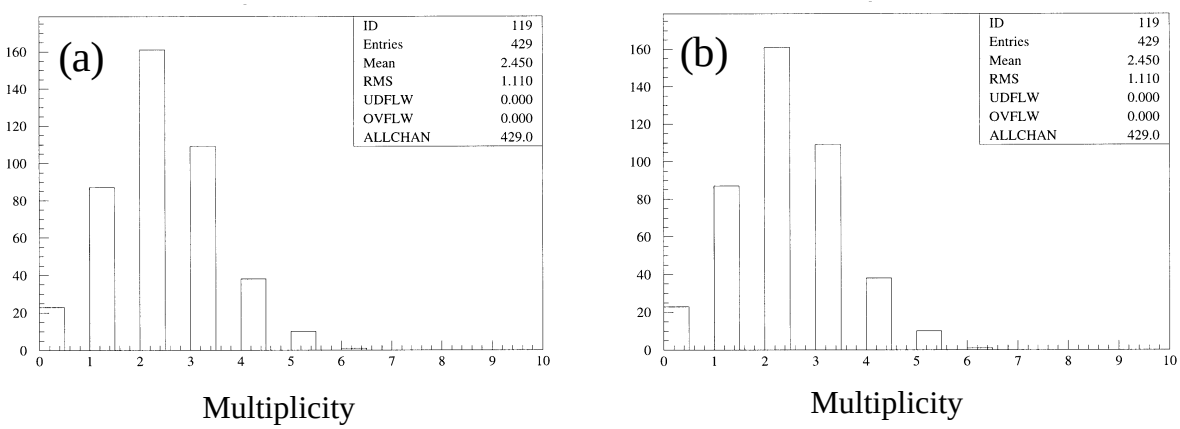


Fig. 14 – Measured multiplicity distribution of the background photon pulses found with the de-convolution algorithm in the time window of 0-30ns using (a) the natural quartz bar with the mirror, and (b) the synthetic fused silica bar with the photon trap.

Table 1 – Data: Most probable number of the background photon pulses found for each single cosmic ray muon passing at an incident angle of 56.5° relative to bar axis, as found by two different algorithms and for two different radiator materials, synthetic fused silica and natural quartz. The natural quartz bar had the mirror, the synthetic fused silica bar had the photon trap in this table.

| Case | Time window [ns] | Number of the background photons per one muon (peak finding algorithm) | Number of the background photons per one muon (de-convolution algorithm) |
|---|---|---|---|
| Natural quartz with the mirror | 0 < time < 30 | 1.9 ± 0.9 | 1.6 ± 1.0 |
| Synthetic fused silica with the photon trap | 0 < time < 30 | 2.2 ± 0.9 | 2.5 ± 1.1 |
| Synthetic fused silica with the photon trap | 0 < time < 70 | 5.0 ± 1.6 | 4.6 ± 1.8 |

## 5. Detailed comparison of the 4m-long bar data with the Monte Carlo.

Figure 15 shows a comparison of the time distribution from the combined data and the Monte Carlo simulation. The time stamp for each entry into the plot was created using the simple peak finding algorithm. The comparison is done only in the very first time interval of 0-30ns, i.e., before the Cherenkov signal arrives (mirror data). The first peak in the data corresponds to the Cherenkov radiation created by the energetic delta ray electrons. The first peak is then followed by the second peak, which is caused by the reflection of the Cherenkov signal photons from the first bar-to-bar joint. The third peak is less noticeable. It is caused by the reflection of the Cherenkov signal photons from the second bar-to-bar joint. The Monte Carlo curve near the first peak is not fit to the data, but shows the predicted absolute number of photons for the corresponding number of tracks. The height of the second and the third peak in the Monte Carlo has been "tuned" empirically with the reflectivity of the EPOTEK-301-2 glue/fused silica interface. This "tuned" reflectivity is shown in Fig. 3. Figure 15 indicates that the Monte Carlo simulation explains the basic features of the data very well. One can see that the MC overestimates somewhat a number of hits in the first peak.

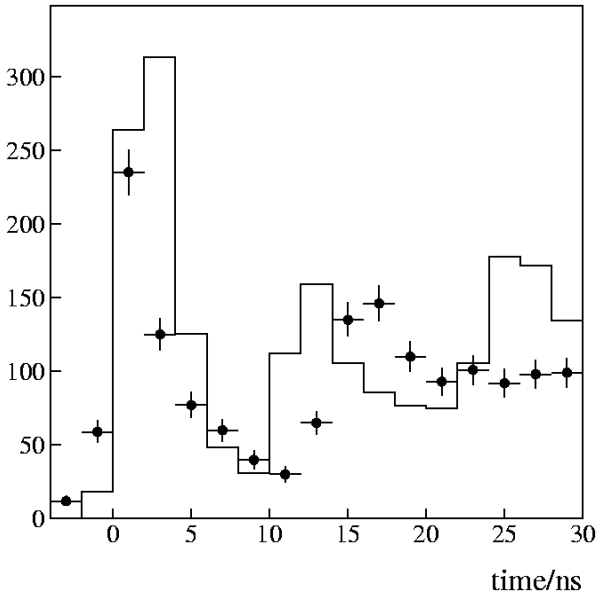


Fig. 15 – Combined data: Time distribution of photon background pulses caused by a muon passing fused silica 4m-long bar at incident angle of 56.5$^{o}$ in the first 30ns after the appearance of the very first background pulse. The data (a combined of both the mirror and photon trap data) is represented by the dots and the Monte Carlo by the smooth line.

Figure 16 shows a comparison between the photon trap data only from the 4m-long bar and the Monte Carlo simulation over the entire available time interval of 0-70ns. The time stamp for each data entry into the plot was created using the de-convolution algorithm in this case. The Monte Carlo simulates the photon arrival as a delta-function in time (no pulse simulation is performed). In this case, the Monte Carlo prediction seems to fade sooner compared to the data, however, again, the basic features are reproduced very well.

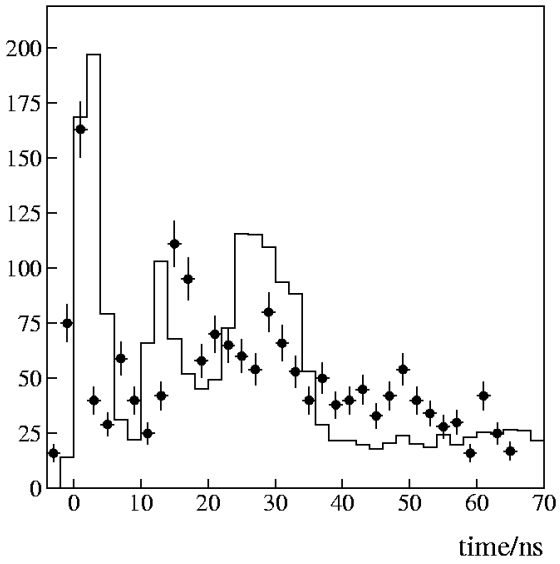


Fig. 16 – Photon trap data: Time distribution of photon background pulses caused by a muon passing fused silica 4m-long bar at incident angle of 56.5° in the first 70ns after the appearance of the very first background pulse. The data are dots and the Monte Carlo prediction is a smooth line.

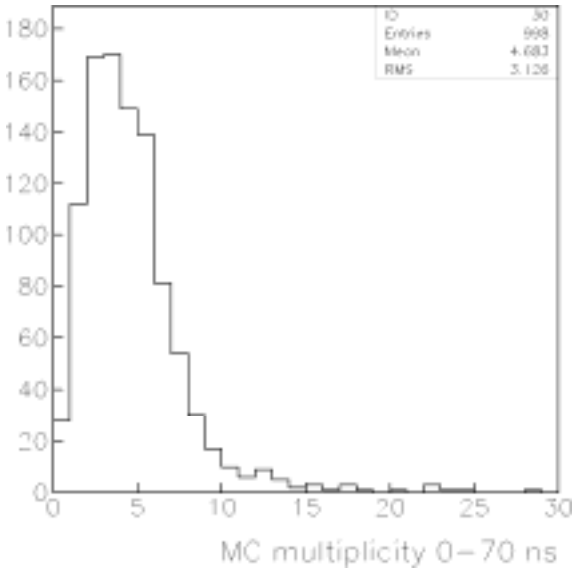


Fig. 17 – Photon trap only case: Monte Carlo prediction of the multiplicity distribution of the background photon pulses caused by a muon passing the fused silica 4m-long bar at incident angle of 56.5° in the time window of 0-70ns. No fudge factor was used in this distribution. The agreement with experimental result shown in Fig. 13 and Table 1 is very good in terms of the most probable number.

Figure 17 shows the Monte Carlo multiplicity distribution of background photon pulses found in the time window 0-70ns for the synthetic fused silica bar equipped with the photon trap. Its most probable value agrees very well with the data shown in Figure 13b, which indicates that the multiplicity of the background photons is $4.6 \pm 1.8$. Of course, in BaBar we do not have the photon trap, and therefore Fig. 17 can be used only to confirm that the simulation in Monte Carlo is realistic because it agrees with the equivalent data. One should point out that the present Monte Carlo does not treat the individual photons as pulses with a finite shaping time, and therefore it tends to enhance a tail in the distributions compared to data.

Figure 18 shows the Monte Carlo prediction for the multiplicity of pulses found in the time window of 0-30ns. This is to be compared to Fig. 14.

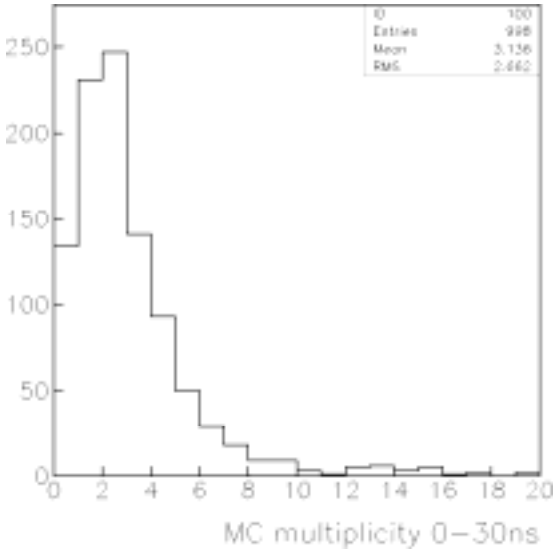


Fig. 18 – Mirror only case: Monte Carlo prediction of the multiplicity distribution of the background photon pulses caused by muon passing the fused silica 4m-long bar at incident angle of 56.5° in the time window of 0-30ns. No fudge factor was used in this distribution. The agreement with experimental result shown in Fig. 14 and Table 1 is reasonable in terms of the most probable number.

In the Monte Carlo, we switch off the Cherenkov signal at the mirror end. Figure 19a shows the multiplicity distribution of all background photon pulses in the time window 0-70ns for the synthetic fused silica. We see that the most probable multiplicity is about five. However, the distribution has a long tail. Figures 19b,c shows the breakdown of this multiplicity count into either the delta-ray contribution only or the Cherenkov signal-induced background from the glue reflections. We expect ~96 photoelectrons from the Cherenkov signal at this dip angle and the time interval. We conclude that the most probable number of background hits represents ~5% compared to the "proper" DIRC Cherenkov signal at this dip angle, however, the distribution has a long tail, i.e., some events have much larger number of background hits.

Up to this point, all comparisons between the test data and the Monte Carlo simulations neglected a contribution from the scintillation. In fact, Fig. 15 indicates that we are explaining data quite well already with this assumption, which is based on our scintillation rate measurements in chapter 3.

It would be, perhaps, of some theoretical interest to investigate if the scintillation would have effect on the result, if we artificially increase the detected rate of the scintillation photons compared to results presented in chapter 3. We want to show that it is not possible to explain the data with just contributions from the delta-rays plus the scintillation alone, as was originally suggested [2,3]. To make this point, we switch off the glue reflections. Figure 20a shows a total multiplicity distribution of the background photons in the time window of 0-70ns for the synthetic fused silica, and Figures 20b,c show breakdown of this multiplicity count into either the delta-ray only or the scintillation only contributions. The scintillation rate is set artificially to be the same as in Fig. 19c, i.e., about four photons per muon, and it is assumed to be distributed randomly along the muon track and with a random photon direction. The result is shown in Fig. 21, which proves that we cannot reproduce the second peak observed in the data. It is clear that one cannot differentiate between the scintillation photons and the delta-ray photons using the timing information. Therefore, the rate of the scintillation photons is determined separately, as described in chapter 3.

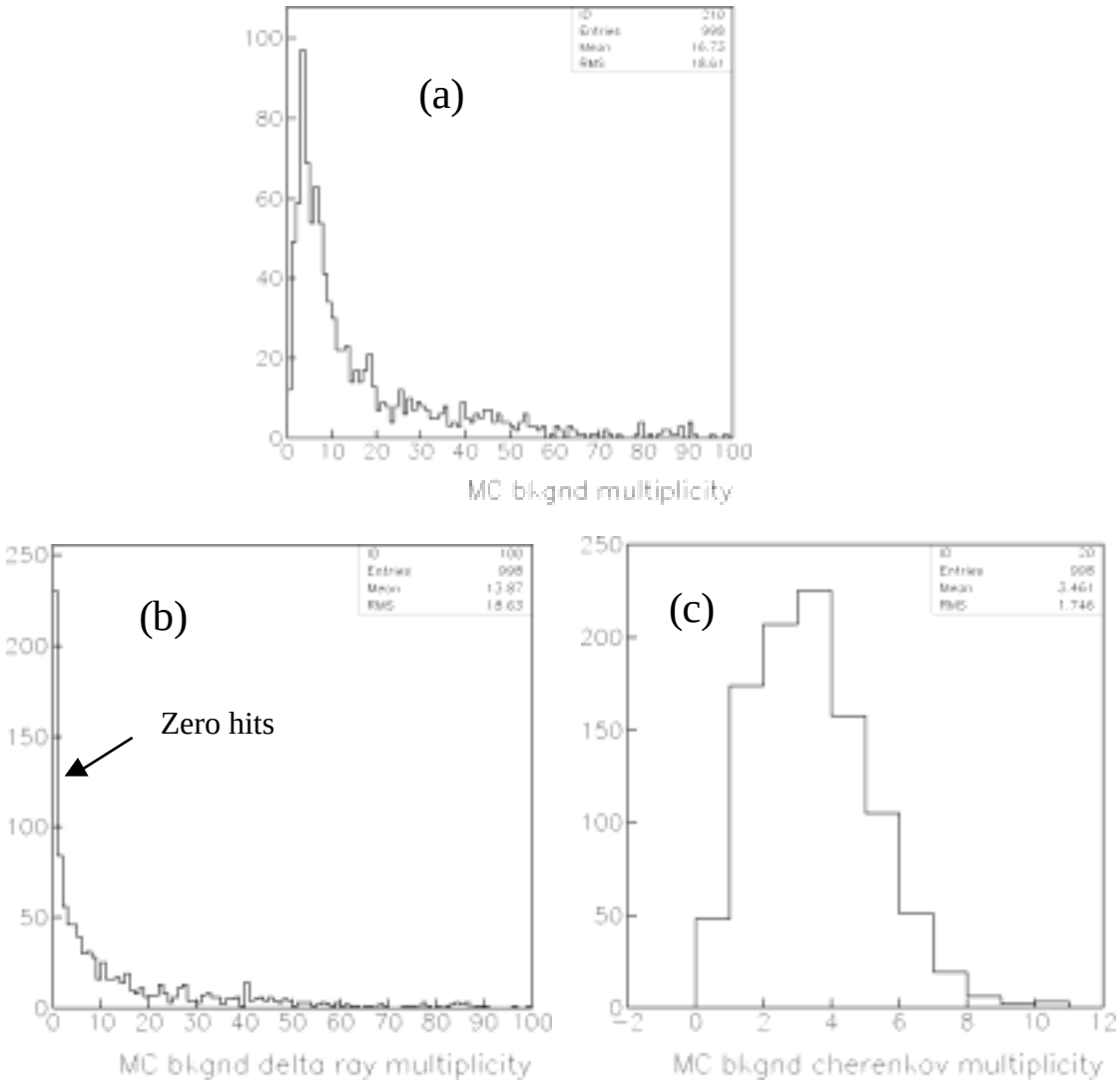


Fig. 19 – Monte Carlo prediction of the multiplicity distribution of the background photon pulses caused by a muon passing the fused silica 4m-long bar at incident angle of 56.5° in the time window of 0-70ns. It is assumed that the background photons, i.e., either the delta-ray induced or the Cherenkov photons reflected from the glue interfaces, are reflected by the mirror, however, all "proper" Cherenkov signal photons are absorbed at the mirror end, so that they do not interfere with the pulse count. This simulates a realistic prediction of the total background multiplicity in the DIRC bar in BaBar, which is, of course, normally obscured by the Cherenkov signal. No fudge factor was used in this distribution. (a) All background photons (one can see that the most probable number of any type of background hit is about five; however, the distribution has a very long tail caused by the delta-ray contribution), (b) the delta-ray-induced background photons only, and (c) the Cherenkov-induced background photons reflected from the glue-fused silica interfaces.

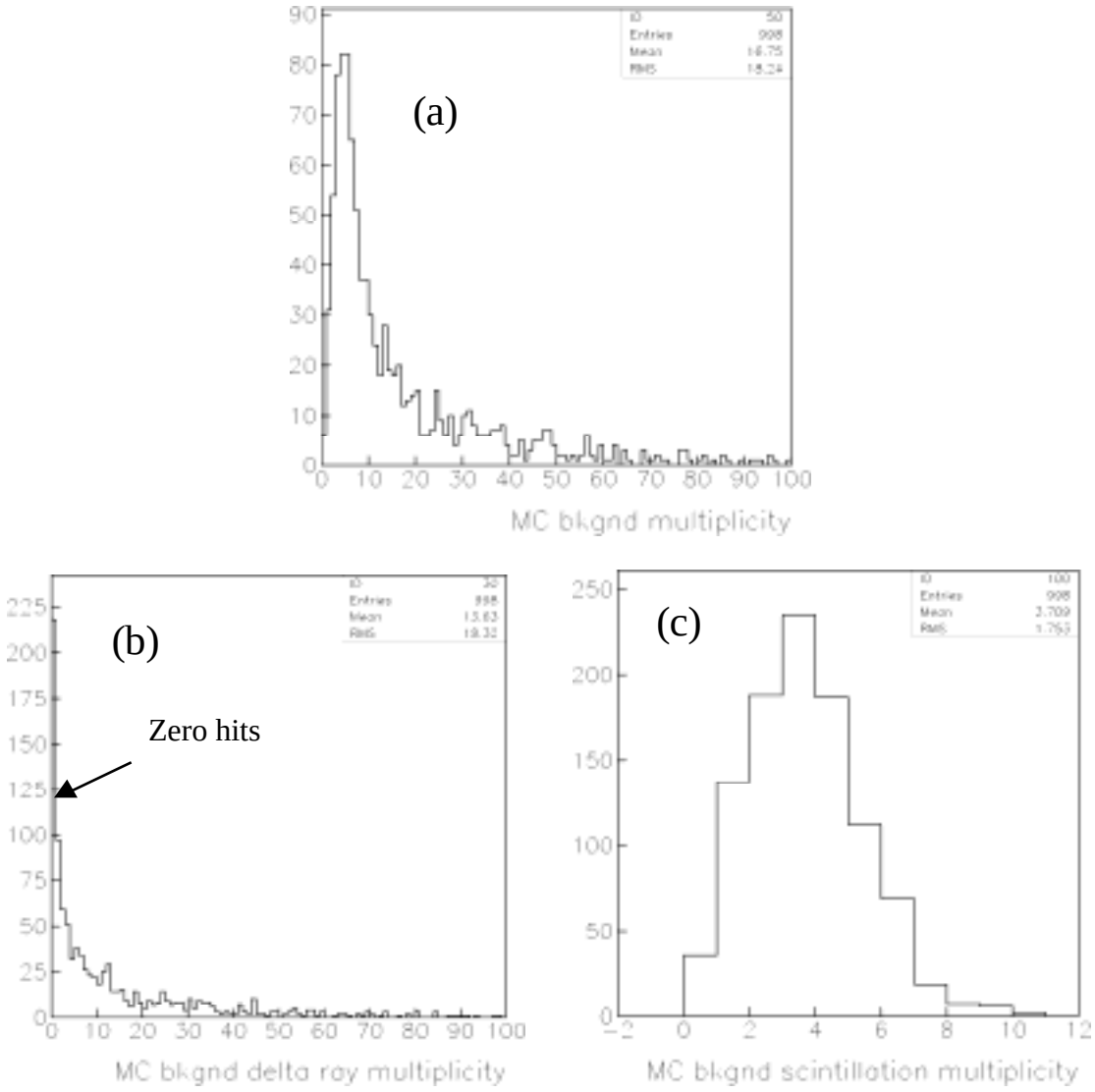


Fig. 20 – Monte Carlo prediction of the multiplicity distribution of the background photon pulses caused by a muon passing the fused silica 4m-long bar at incident angle of 56.5$^{o}$ in the time window of 0-70ns. It is assumed that the background photons, i.e., either the delta-ray induced or the scintillation photons, are reflected by the mirror, however. No fudge factor was used in this distribution. (a) All background photons (one can see that the most probable number of any type of background hit is about five; however, the distribution has a very long tail caused by the delta-ray contribution), (b) the delta-ray-induced background photons only, and (c) the scintillation background photons only (multiplicity adjusted to agree with that of Fig. 19c).

Finally, we will try to explain the data using all three contributions assuming that the scintillation rate is artificially increased by a factor of five compared to the experimental results presented in chapter 3. We will try to explain the photon background data using three contributions: (a) the delta ray-generated Cherenkov photons, (b) the scintillation rate of ~0.6photons/muon (5 times larger than what was measured in chapter 3) and (c) the Cherenkov photons, which reflected back from the glue/fused silica interfaces. We tune the reflectivity of the glue/fused silica interface to get agreement between the data and Monte Carlo on the second peak..

We eliminate the scintillation mechanism from our problem using two arguments, (a) one that the experimental results of chapter 3 show that the scintillation rate is negligible, and (b) second that Monte Carlo explains the test data very well without a need to introduce the scintillation (Fig. 15).

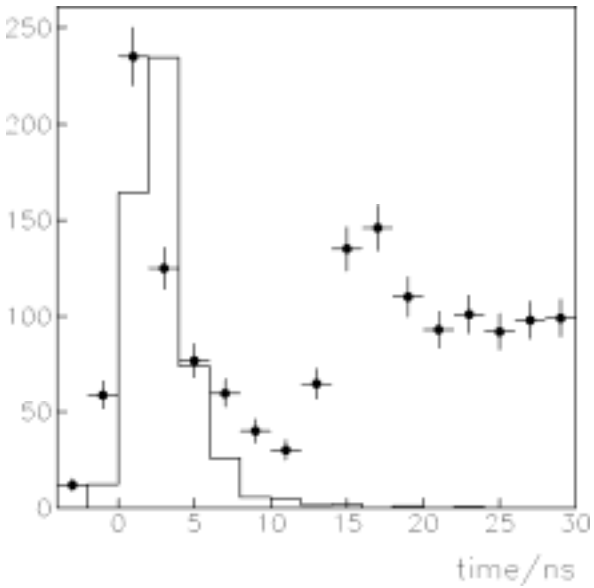


Fig. 21 – Combined data: An attempt to explain the data shown in Figure 15 using the delta ray and the scintillation mechanisms only, i.e., the Cherenkov photons do not participate via the reflection mechanism. The data are crosses, the Monte Carlo prediction is a smooth line. The reflections from the glue/fused silica interfaces were switched off. The scintillation rate was adjusted to be the as that of Fig. 19c. Since number of MC events in the first peak would be overestimated, we apply a fudge factor of 0.45 to get an agreement with the data.

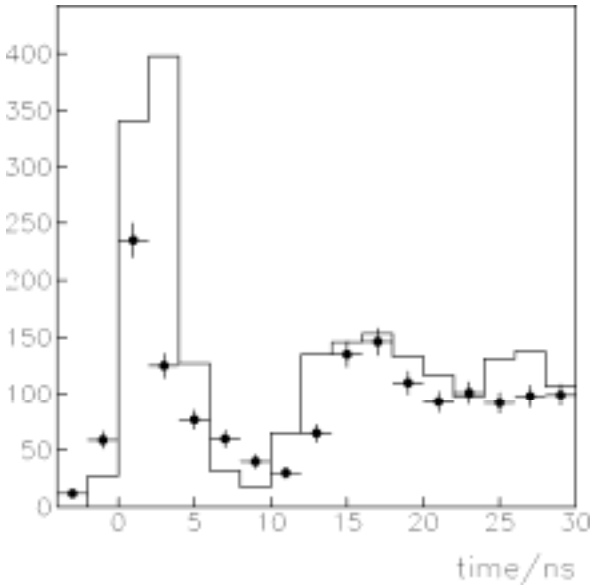


Fig. 22 – Combined data: An attempt to explain the data shown in Figure 15 using all three mechanisms, i.e., using the delta ray, the scintillation (~0.6 photons/muon ~ 5 times larger rate than what was measured in chapter 3) and the reflected Cherenkov photon. The data are crosses, the Monte Carlo prediction is a smooth line. Because of the addition of the scintillation, the reflection coefficient had to be adjusted (curve #2 in Figure 3).

# 6. Monte Carlo Program developed for this study.

We started from a FORTRAN Monte Carlo program "DIRC Bar Simulation" which already had a basic simulation of the Cherenkov photon production, photon propagation through the bar geometry, including the PMT detection. In this program, photons are emitted randomly along the track of the traversing charged particle. The wavelength dependent production of the Cherenkov photons follows the equation given by Ref. 6. It gives a total number of photons $N_0 = 1450$ for a wavelength of $\lambda = 400$nm and a dip angle of about $56.5^0$. The acceptance of the photon is given by the quantum of the photomuliplier. The quantum efficiency is obtained from the Electron Tube Ltd. Photons are generated with random polar Cherenkov angles $\Phi_c$ with respect to the track. The wavelength dependence of the Cherenkov angle $\Theta_c$ enters via the refraction index $n = n(\lambda)$ of fused silica, which was provided by the fused silica manufacturers.[4] The photons are transformed into the bar coordinate system. If the photon vector hits one of the six surfaces the algorithm decides on base of the refraction index if the photon is reflected or exits the bar. The program successively bounces photons through the bar allowing for the incorporation of detailed effects such as scratches, chips or other deterioration along the bar. If the photon reaches the mirror end, it is reflected.

For a photon reaching the readout end a total survival probability is calculated as a product of:

- attenuation in fused silica bulk material was assumed to be 0.997 per meter
- internal reflection coefficient value of 0.99968 per bounce was used
- mirror reflectivity value of 0.937 was used.

In the following we describe additions to the "DIRC Bar Simulation" by the present effort.

## 6.1. Production of Delta Ray Electrons Using the FLUKA Program.

When a muon passes through the fused silica bar, among the many interactions that take place is the generation of delta rays. Some of these delta rays (electrons) are traveling at speeds that are greater than the phase velocity of light in fused silica and so generate their own Cherenkov photons, which belong to a category of the background photons. We generate these electrons using the FLUKA (FLUcuating Kaskade) program [7].

FLUKA determines how long a particle travels before an interaction takes place. For particles in which the cross sections is constant between two consecutive processes, the interaction points are exponentially distributed as:

$$P(x) = \sum_{tot} e^{-\sum_{tot} x}$$

where sigma is the total macroscopic cross section and is given by

$$\sum_{tot} = \sum_{i=1}^{n} \frac{N_A \rho_i}{P_{Ai}} [\sum_{j=1}^{k} \sigma_{ij}(E)] + \frac{m}{p\tau}$$

Here the first sum over *i* is for the different types of atoms that are present in a given material ($N_A$ is Avogadro's number, $\rho_i$ is the partial density, and $P_{Ai}$ is the atomic weight of the atom of type *i*). The second sum is for the *k* possible kinds of interactions. As usual, $\sigma_{ij}$ (E) is the microscopic cross section pertaining to the *i* atom and the *j* kind of interaction. The second term in the equation is the macroscopic decay cross section, where *m* is the mass of the object, *p* is the momentum, and $\tau$ is the mean lifetime.

Once the interaction point is determined, the kind of process must be computed according to the relative probabilities $\Sigma_{ij}/\Sigma_{tot}$ for atomic/nuclear interactions and $\Sigma_d/\Sigma_{tot}$ for decay. However, for charged particles the situation is more complicated because the cross section changes between two consecutive interactions. The

[4] Refractive index of Suprasil, Heraeus Amersil Inc., USA. It was checked that it agrees with the Melles-Griot Optical Co. formula used in Fig. 1 of chapter 2.

solution that is adopted is to sample the interaction points according to the above equation, but instead of using the macroscopic cross section that corresponds to the particle being at the beginning of the step, it uses the maximum value of the macroscopic cross section along the step length. Then, its new energy and total cross section will be completed determined by the processes that occurred during the step. This interaction, which is initially picked at random, is accepted with the probability

$$P_{acc} = \frac{\sum_{tot}(E_{new})}{\sum_{\max}}$$

This algorithm (called the "fictitious sigma") method is an example of a rejection method, which can be used to exactly distribute the interaction points. Once the interaction point is sampled and a delta ray is chosen as the type of interaction, the kinetic energy of the knock on electron is chosen according to the cross section given by

$$\left(\frac{d\sigma}{dT_e}\right)_{\frac{1}{2}} = \frac{2\pi\, z^2\, r_e^2\, m_e\, c^2}{\beta^2\, T_e^2}\left[1-\beta^2\frac{T_e}{T_{\max}}+\frac{1}{2}\left(\frac{T_e}{T_o+Mc^2}\right)^2\right]$$

were T-max is the maximum kinetic energy transfer to the electron determined by kinematics. It is defined as follows:

$$T_{\max} = \frac{2\, m_e\, c^2\, \beta^2\, \gamma^2}{1+2\gamma\frac{m_e}{M}+\left(\frac{m_e}{M}\right)^2}$$

Although the muon energy was not fixed in this test, a lower limit can be estimated because the particle must traverse through about ~30 cm of lead before triggering the bottom scintillator (see Fig. 5). Using an average value of the dE/dx for lead (1.123 MeV/g/cm2), one can calculate the minimum muon energy as approximately ~0.4 GeV. A value of about 2 GeV, and a muon angle of 56.5°, was used as an input to FLUKA. The procedure, therefore, is to have FLUKA produce tracks through the quartz bars. Then a file is created with all the necessary information that can be used in the Monte Carlo simulation of the bars. Even though the above two numbers (energy and angle) were used in the majority of simulations, several different energies (0.4 and 100 GeV) and angles (61 and 51 degrees) were also simulated to understand how the simulation results varied when these two parameters were changed.

## 6.2. Delta Ray Treatment in the Monte Carlo.

The MonteCarlo program first reads the data generated by FLUKA, it then decides which electrons are above the Cherenkov threshold (typically ~4 per each muon). It then proceeds to transport these electrons through the fused silica bar until their energy falls below the Cherenkov threshold. The stepping is done in small 3μm-long steps and energy is degraded using the Bethe energy loss formula [8], and it also included the multiple scattering [8, 9]. If a photon is emitted in a given step, the program determines the Cherenkov angle and the corresponding direction cosines. One should say that the addition of the multiple scattering had little effect on our results. The delta rays are responsible for the first peak appearing in time spectrum of Fig. 15.

### 6.2.1. New effects added since the version of this note from Sept. 19, 2001.

Previous version of our Monte Carlo program did not take into account the secondary electron interactions, such as are bremsstrahlung and Moller scattering, properly. The main effect of this problem was to generate more photons than expected. To rectify the problem, one had to determine which delta ray had a secondary interaction and do proper accounting of all electron track segments to create the correct amount of the Cherenkov radiation. As one might imagine, this reduced the number of photoelectrons recorded in the PMT. Previously, one had to normalize the Monte Carlo to the data with an arbitrary fudge factor, but now this is not

necessary any more. In addition, the curve for the reflection probability changed, making it more in agreement with the Fresnel theory.

## 6.3. Basic wavelength-dependent effects

We have included the absolute wavelength dependency of the internal reflection coefficient, mirror reflectivity according to Ref. 4. The wavelength dependency of the photon attenuation in the bulk material of fused silica was taken from Ref. 10.

## 6.4. Simulation of Glue / Fused Silica Interfaces.

The next step is to understand why there is the second peak in Fig. 15, which appears before arrival of the Cherenkov signal. It was thought that this could be the result of reflection from the glue/fused silica interfaces due to the difference in the respective refraction indices. We tried two methods of calculations: the first one was based on our measurement of the refraction index and the second one was based on a direct measurement of the reflectivity from the glue/fused silica interface [4].

Let's first discuss the first method. A fit to our data of the refraction index is

$$n_e = -3.09 \times 10^{-9}\ \lambda^3 + 5.25 \times 10^{-6}\ \lambda^2 - 3.07 \times 10^{-3}\ \lambda + 2.18$$

where $\lambda$ is given in nm. Figures 23 and 24 show the simulated distribution based on this dependency assuming the Fresnel reflection theory, one assuming TM mode and the other TE mode of reflection. In Fig. 23 (TM mode) there a second peak at approximately 10ns after the first and a third at approximately 25ns. In the data (see Fig. 15), the time between the first and second is about 15ns, while the third is not measured well. An important number is the ratio between the first and second peaks (defined as ratio of the peak integrals over the ranges between 0-10ns and 10-20ns of the histogram in Fig. 23). This number is 7.03, while in the data it is approximately 1.1, i.e., the second peak is much more pronounced in data. Figure 24 shows the same simulation assuming the TE mode reflection (the E-field vector perpendicular to the plane of incidence). Notice that the deep valley between the second and the third peaks is more pronounced in the TM mode compared to the TE mode. In the data (see Fig. 15) we have, of course, contributions from modes.

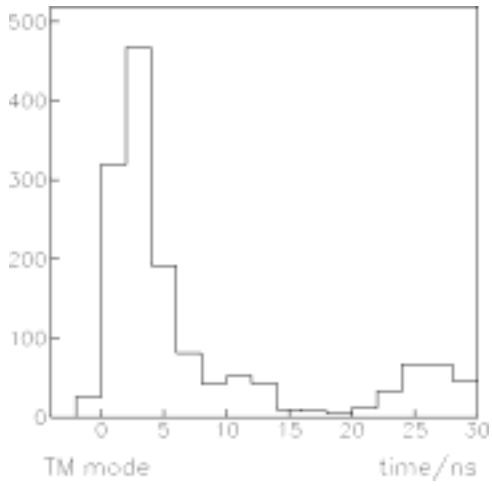


Fig. 23 – Monte Carlo: A histogram of the number of photoelectrons in the DIRC bar generated indirectly by the passing muon and subsequent delta rays. Delta ray photons account solely for the first peak, and the last two peaks result from the reflection from glue/fused silica interfaces. The glue reflection is modeled by Fresnel's theory using the TM mode (E-field vector parallel to the plane of incidence). The time between the first and second peak is about 10ns and the ratio between the first and second (defined as the ratio of the integral between 0-10ns and 0-20ns) is 7.03. These numbers should be compared to data, which are 15ns and 1.1.

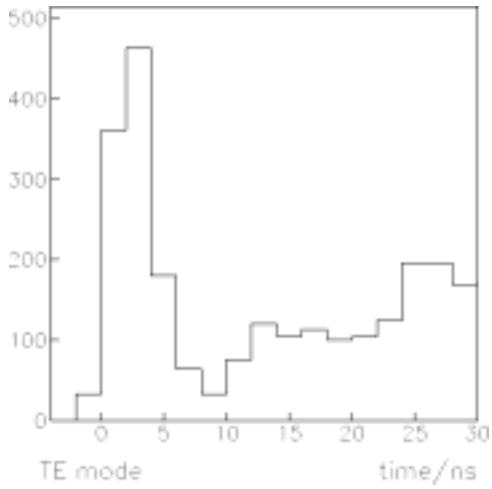


Fig. 24 – The glue reflection is modeled by Fresnel's theory using the TE mode (E-field vector perpendicular to the plane of incidence). In this histogram, the valley is absent as a result of the qualitative difference between the TE and TM mode curves. The time between the first and second peak is about 10ns and the ratio between the first and second is 1.97.

Finally, the most accurate reflection model was developed in which the polarization vector was determined at the photon's creation and carried through as the photon propagates down the bar. Therefore, when the photon hits the glue planes, the reflection probability is determined by a linear combination of TE and TM modes. The result of this simulation is shown in Fig. 25.

Up to this point the reflection on the glue/fused silica interface was calculated using the Fresnel reflection theory using our measured refraction index [4]. However, we have also measured this reflection directly at the wavelength of 442nm (for TE mode) [4]. Using this measured result and normalizing it to the reflection probability at zero degree incident angle as calculated by the Fresnel theory, one obtains a polynomial fit to the data as follows:

$$reflection\ probability = 1.56 \times 10^{-5}\theta^2 - 8.8 \times 10^{-5}\theta + 1.44 \times 10^{-3}$$

Figure 26 uses this reflection probability to obtain the time spectrum in MC.

The peak corresponding to the first glue/fused silica interface is now at approximately 14ns, and also the amount of photons reflecting from the first and second glue planes is greatly increased compared to the Fresnel theory discussed so far. It is evident that the result of the shift is due to the fact that more photons at steeper incident angle are being reflected.

In the final simulation, which is shown in Fig. 22, we used a scintillation rate of 0.6 photons/track (see chapter 3). After some empirical tuning of the 1-st coefficient, the reflection probability from the glue/fused silica interface was found to be the following:

$$reflection\ probability = 0.75 \times 10^{-5}\theta^2 - 8.8 \times 10^{-5}\theta + 1.44 \times 10^{-3}$$

Based on Fig. 22, we conclude that the simulation of the timing spectrum agrees well with the data as far as the normalization of the second peak. However, the time between the first and second peaks is about 1 to 2 ns off from the data, and this discrepancy was never really satisfactorily explained.

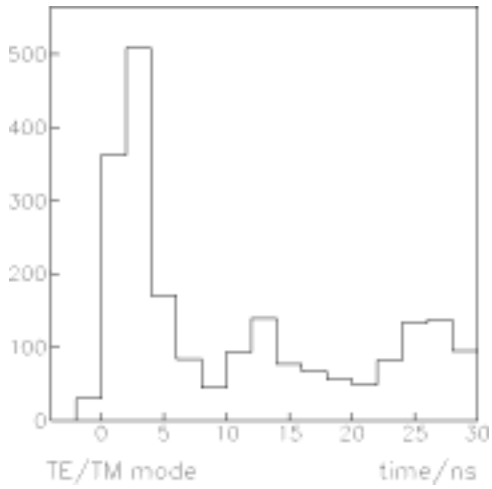


Fig. 25 – The photon polarization vector is carried with the photon as it propagates down the bar. When it encounters a glue plane, an appropriate linear combination of TM and TE modes are taken. This histogram has the same 10 ns separation between peaks and a ratio between the first two peaks of 3.106.

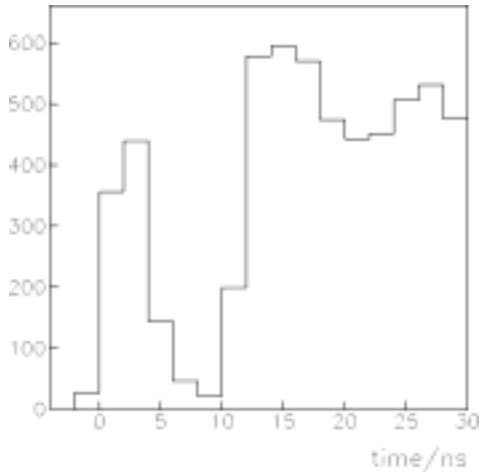


Fig. 26 – Instead of using Fresnel theory to model the reflection from glue, this histogram is a result of using data from an independent experiment that measured reflection from the glue [4]. A polynomial fit was obtained to the data and inserted into the Monte Carlo program. The amount of photons reflecting from the first glue plane is greatly increased, and in fact ratio of the first and second peaks is .528, which is an overshoot as compared to the data. However, the timing is improved, as now the time separation of the first two peaks is 14ns.

## 6.5. Group Velocity.

We use group velocity to determining the arrival of time the photon at the PMT was used:

$$v_{gr} = v_{ph}\,(1+\frac{\lambda}{n}\frac{dn}{d\lambda})$$

This had a significant effect for a long propagation times above ~35ns.

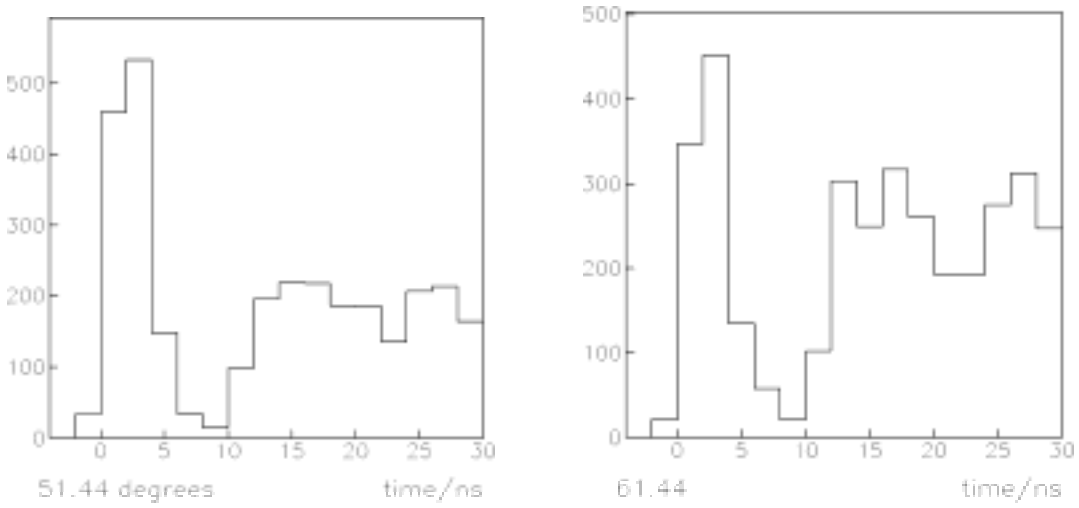


Figs. 28 - The muon entrance angle was changed to the specified values. Both timing and the ratio of peak values of the 1-st and the 2-nd peak are somewhat sensitive to the angle change.

## 6.6. Variation of Muon Angle.

The muon angle was changed by 5$^o$ to check the results if the measurement would have such systematic error. The expected statistical error in angle is less than 1$^o$. Figure 28 shows a result of running at two incident angles of 61.44$^o$ and 51.44$^o$. It is interesting to note that the number of photons coming into the PMT is significantly affected, but the actual time is not.

## 6.7. Variation of Muon Energy.

In addition to the muon energy of 2 GeV, two other energies (.4 and 100 GeV) were simulated. The lower limit of 0.4 GeV was chosen because this was the minimum energy that could trigger the counters. An upper limit of 100 GeV was chosen because this was a reasonable upper bound on the energy of muons at the earth surface. Figure 29 shows that the change of muon energy did not significantly affect the results.

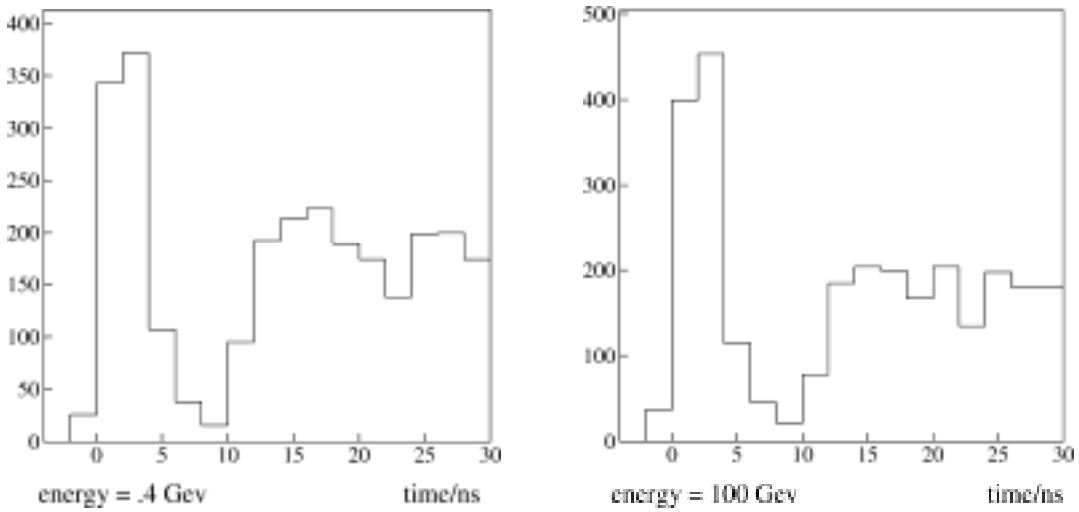


Figs. 29 - The muon energy was changed to the specified values. Both timing and the ratio of peak values of the 1-st and the 2-nd peak are insensitive to this change.

## 7. Comparison of Data and Monte Carlo Program in BaBar.

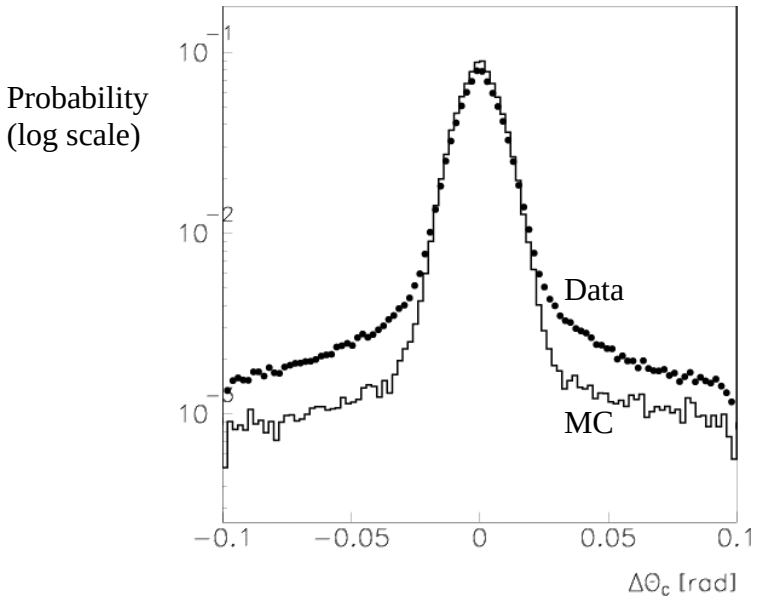


Figs. 30 - The single photon Cherenkov angle distribution for muon tracks from the reaction $e^+e^- \rightarrow \mu^+\mu^-$ as reconstructed in the BaBar DIRC (dots) and the Monte Carlo prediction using the "official" DIRC MC program, which includes the delta rays only (no scintillation or glue reflections). It does not have the improvements mentioned in this note.

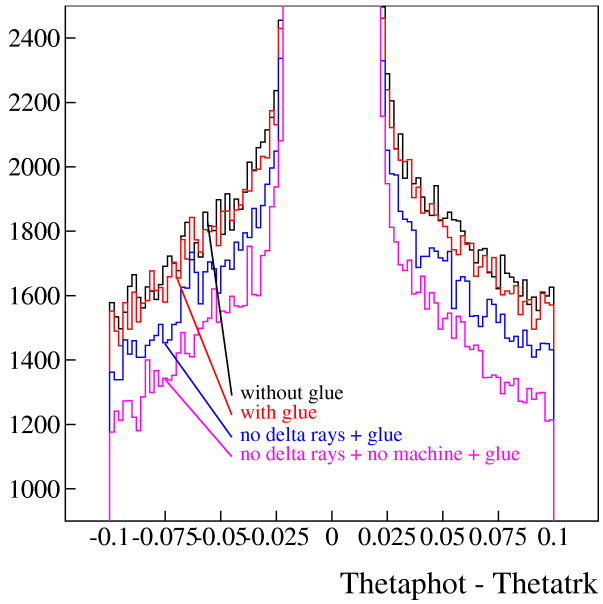


Figs. 31 – The effect of various contributions on the MC tail distribution of the single photon solutions of the Cherenkov angles in BaBar muon tracks.

Figure 30 shows the single photon Cherenkov angle distribution for muon tracks from the reaction $e^+e^- \rightarrow \mu^+\mu^-$ as reconstructed in the DIRC of BaBar. Combinatorial background is removed by requiring that a photon lies closest to the expected Cherenkov angle and arrival time. The remaining background under the signal peak

contributes up to 15%. Only about 60% of the background level is presently explained by the BaBar DIRC Monte Carlo. The only significant contribution is generated by delta rays. However, one should point out that we have used in this work the FLUKA [7] generator to simulate the delta rays. It remains to be yet seen if the BaBar generator of the delta rays and their subsequent use to generate the Cherenkov photons is equivalent to our procedure. The BaBar DICR Monte Carlo does not foresee scintillation in the quartz presently. We have shown in this work that a significant source of secondary light in addition to delta ray is the reflection of Cherenkov photons on glue joints with actual comparable size. We have demonstrated experimentally that the scintillation contribution is negligible, and it is not necessary to explain our data.

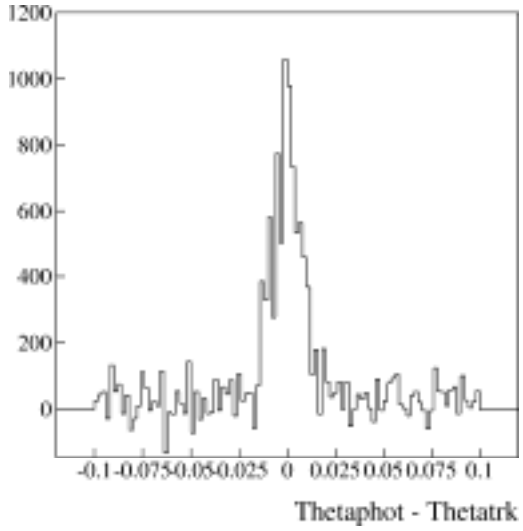


Figs. 32 – The MC distribution for the single Photon solutions of the Cherenkov angles in BaBar muon tracks. The graphs show a difference distribution between glue reflection "in" and "out" (the glue "removes" ~3.1% of photons in the Cherenkov peak area only).

We added glue reflection to the "official" DIRC BaBar MC program now, as motivated by this work. Figures 31 and 32 show the effect of the glue reflection on the BaBar DIRC MC distribution of the single photon solutions for the Cherenkov angles and time of arrival in muon tracks from the reaction $e^+e^- \rightarrow \mu^+\mu^-$ as reconstructed in the DIRC of BaBar.

However, the BaBar DIRC MC program does not include the "Fluka way" of generating photons, as well as many other improvements described in this note.

# Conclusions

- We show experimentally that the scintillation mechanism induced by passing muon is negligible in DIRC fused silica bars. It represents less than 1% of total photon background in the fused silica bar.
- Instead, we argue that there are two other major components in the DIRC photon background. One component consists of photons created by the delta-ray electrons in the fused silica, which in turn produces the Cherenkov light. The second component comes from the reflections of all photons from the EPOTEK-301-2 glue/fused silica interfaces. The reflection occurs because of a slight mismatch of the refraction index between the optical glue and the fused silica.
- We conclude that the most probable number of background hits represents ~5% relative to the number of the "proper" DIRC Cherenkov photon measured at a dip angle of 56.5$^o$. However, the distribution has a long tail due to the delta-ray contribution, i.e., some events have much larger number of background hits.
- The note will be useful to estimate the photon background multiplicity and provides a recipe how to simulate it in the BaBar Monte Carlo for each passing minim-ionizing particle through the DIRC bar.

# Acknowledgements

We would like to thank B. Ratcliff for interest and several suggestions related to this study. A technical help to create the experimental setup of R. Reif and M. McCulloch was very much appreciated. Contributions in initial phases of J. Shaewitz are also valued. We appreciate a help of M. Krishnamurty to generate Fig.30, and D. Aston to generate Fig.31.

# References

1. B. Ratcliff, SLAC-PUB-6047, January, 1993.
2. M. Benkebil and G. Warmser, BaBar DIRC Note #125, July 1, 1999.
3. S. Plaszczynski, Habilitation Thesis, April 10, 2001.
4. J. Va'vra, BaBar DIRC Note #140, July 15, 2001.
5. J.Va'vra, BaBar DIRC Note 129, April 12, 2000.
6. J.D. Jackson, Classical Electrodynamics, 2-nd edition, John Wiley & Sons, N.Y. (1975).
7. A. Fasso, A. Ferrari, J. Ranft, FLUKA99 program.
8. H. Bethe, Physical Review, Vol. 89, Number 6, March 15, 1953, page 1256.
9. The EGSH Code System, SLAC-Report-265, December 1985.
10. H. Krueger, R. Reif, X. Sarazin, J. Schwiening and J. Va'vra, BaBar DIRC Note #40, May 20, 1996.
11. We appreciate a help of M. Krishnamurty to generate this plot.